molecules

MDPI

Article

Role of Stereochemistry on the Biological Activity of Nature Inspired 3-Br-Acivicin Isomers and Derivatives

Andrea Galbiati[1,#], Aureliano Zana[1,#], Chiara Borsari[1], Marco Persico[2], Stefania Bova[4], Oleh Tkachuk[2], Alexandra Ioana Corfu[1], Lucia Tamborini[1], Nicoletta Basilico[5], Caterina Fattorusso[2], Stefano Bruno[3], Silvia Parapini[6], Paola Conti[1,*]

[1] Department of Pharmaceutical Sciences, University of Milan, Via Mangiagalli 25, 20133 Milano, Italy; andrea.galbiati@philochem.ch (A.G.); aureliano.zana@philochem.ch (A.Z.); chiara.borsari@unimi.it (C.B.); ioana.corfu@unimi.it (A.I.C.); lucia.tamborini@unimi.it (L.T.); paola.conti@unimi.it (P.C.)
[2] Department of Pharmacy, University of Naples "Federico II", Via D. Montesano 49, 80131 Napoli, Italy; m.persico@unina.it (M.P.); olotuk.6@gmail.com (O.T.); caterina.fattorusso@unina.it (C.F.)
[3] Food and Drug Department, University of Parma, 43124 Parma, Italy; stefano.bruno@unipr.it (S.Br.)
[4] Department of Medicine and Surgery, University of Parma, 43124 Parma, Italy; stefania.bova@unipr.it (S.Bo.)
[5] Department of Biomedical, Surgical and Dental Sciences, University of Milan, Via Pascal 36, Milano, 20133, Italy; nicoletta.basilico@unimi.it (N.B.)
[6] Department of Biomedical Sciences for Health, University of Milan, Via Pascal 36, Milano, 20133, Italy; silvia.parapini@unimi.it (S.P.)
* Correspondence: paola.conti@unimi.it (P.C.); Tel.: +39 02 50319329

Abstract: Chiral natural compounds are often biosynthesized in an enantiomerically pure fashion and stereochemistry plays a pivotal role in biological activity. Herein, we investigated the significance of chirality for nature-inspired 3-Br-acivicin (3-BA) and its derivatives. The three unnatural isomers of 3-BA and its ester and amide derivatives were prepared and characterized for their antimalarial activity. Only the (5*S*, αS) isomers displayed a significant antiplasmodial activity, revealing that their uptake might be mediated by the L-amino acid transport system, which is known to mediate acivicin membrane permeability. In addition, we investigated the inhibitory activity towards *Plasmodium falciparum* glyceraldehyde 3-phosphate dehydrogenase (*Pf*GAPDH), since it is involved in the multitarget mechanism of action of 3-BA. Molecular modelling shed light on the structural and stereochemical requirements for an efficient interaction with *Pf*GAPDH, leading to covalent irreversible binding and enzyme inactivation. While stereochemistry affects the target binding only for two subclasses (**1a-d** and **4a-d**), it leads to significant differences in the antimalarial activity for all subclasses, suggesting that a stereoselective uptake might be responsible for the enhanced biological activity of the (5*S*, αS) isomers.

Keywords: stereochemistry; 3-Br-acivicin; *Plasmodium falciparum*; glyceraldehyde 3-phosphate dehydrogenase; multitarget; covalent inhibitors

Citation: To be added by editorial staff during production.

Academic Editor: Firstname Lastname

Received: date
Accepted: date
Published: date

1. Introduction

Natural products (NPs) have historically played a major role in drug discovery [1], and have been pinpointed as privileged scaffolds for interacting with protein drug targets [2]. The unique chemical diversity and structural complexity of NPs allowed the expansion of the known chemical space explored by medicinal chemists [3]. The majority of NPs are chiral and they are biosynthesized in an enantiomerically pure fashion [4]. Generally, stereochemistry has a crucial impact on drug action, since it affects target binding, metabolism and distribution. For different compounds classes, stereochemistry is the driver for potency and pharmacokinetics [5]. In addition, it has been shown to affect the protein

transport systems resulting in a stereospecific uptake of drugs, as described for β-lactam antibiotics [6].

The natural compound (5*S*, α*S*) acivicin (AT-125, Figure 1A), produced by *Streptomyces sviceus*, and its synthetic analogue 3-Br-acivicin (3-BA, **1a**, Figure 1A) have been described as L-glutamine analogues capable of irreversibly inhibiting several glutamine-dependent amidotransferases, including CTP synthetase (CTPS), carbamoyl phosphate synthetase and XMP aminase [7-9], and γ-glutamyl transpeptidase [10]. The acivicin/3-BA covalent mechanism of action involves the nucleophilic attack of an activated catalytic cysteine residue of the target enzyme to the Cl/Br-substituted C-3 of the 4,5-dihydroisoxazole ring (Figure 1C) [11,12]. Considering the inhibitory activity towards *Trypanosoma brucei* CTPS, 3-BA was 3-fold more potent than acivicin, highlighting that the leaving group plays an important role in the irreversible mode of action. The differences in enzyme inhibition translated into an enhanced *in vitro* and *in vivo* antitrypanosomal activity for 3-BA [13]. Considering different targets, we had previously reported that acivicin was inactive towards *Plasmodium falciparum* glyceraldehyde 3-phosphate dehydrogenase (*Pf*GAPDH), while 3-BA was able to irreversibly inhibits *Pf*GAPDH, a key enzyme of the *Plasmodium* glycolytic pathway [14]. In the erythrocytic stages, the malaria parasite relies heavily on anaerobic glycolysis for energy production [15], leading to the identification of glycolytic enzymes as promising targets for the development of antimalarial agents.

We had previously modified the amino acidic portion of **1a** and synthesized a series of analogues, keeping the stereochemistry of the natural product unchanged. The ester (**2a**, **3a**) and amide (**4a**) derivatives of 3-Br-acivicin were investigated for their antimalarial activity on *P. falciparum* cultures and for the ability to covalently inhibit *Pf*GAPDH. All compounds (**1a-4a**) showed antiparasitic activity against D10 (chloroquine sensitive) and W2 (chloroquine resistant) strains of *P. falciparum*, with IC_{50} lower than 1 μM (Figure 1B). The methyl and benzyl esters displayed the highest second-order rate constant (k_{inact}/K_i) used to characterize covalent binding of irreversible inhibitors to *Pf*GAPDH (**2a**: 10.7; **3a**: 6.6 $M^{-1}\cdot s^{-1}$; Figure 1B) [14,16]. These outcomes clearly indicated that the similarity with L-Gln was not essential for the inhibition of GAPDH.

Despite chemical modifications in the amino acidic portion of **1a** had been extensively explored [14,16-18], the effect of stereochemistry on the biological recognition processes, protein binding and antiparasitic activity has not been investigated yet. Herein, we disclosed the synthesis of the unnatural isomers of **1a-4a**, and we explored the importance of stereochemistry for the *in vitro* antimalarial activity and the inhibitory activity towards recombinant *Pf*GAPDH, which is known to be involved in the multi-target mechanism of 3-BA.

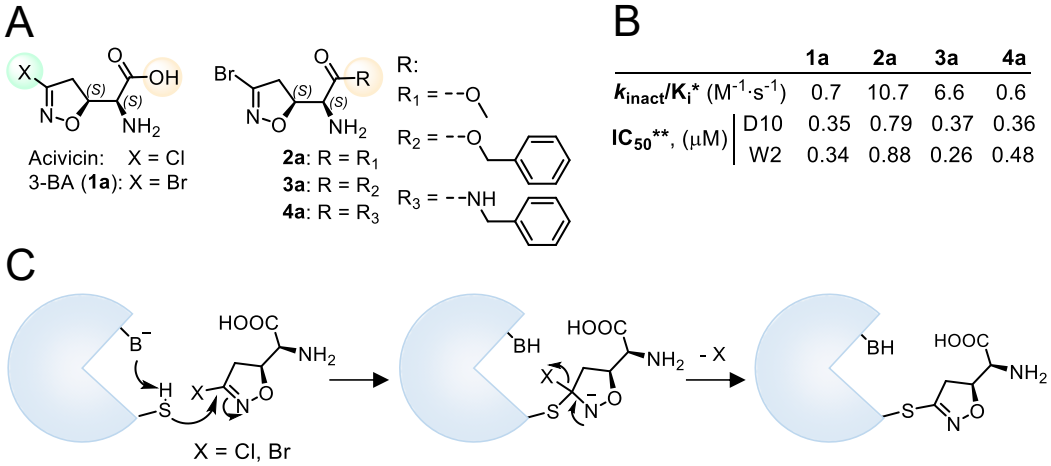

		1a	2a	3a	4a
k_{inact}/K_i* ($M^{-1}\cdot s^{-1}$)		0.7	10.7	6.6	0.6
IC_{50}**, (μM)	D10	0.35	0.79	0.37	0.36
	W2	0.34	0.88	0.26	0.48

Figure 1. (**A**) Chemical structure of acivicin, 3-BA (**1a**) and 3-BA derivatives (**2a-4a**). (**B**) Biological data for compounds **1a-4a**. *Second-order rate constant used to characterize covalent binding

of irreversible inhibitors to *Pf*GAPDH. **IC_{50} towards *P. falciparum* D10 and W2 strains. (**C**) Proposed reaction mechanism for the 3-halo-4,5-dihydroisoxazole moiety.

2. Results and Discussion

2.1. Synthesis of Enantiomerically Pure Unnatural Isomers

The synthesis of the enantiomerically pure target compounds started using the chiral synton (*S*)-**12** or (*R*)-**12**. The diastereoisomeric mixtures **5** and **6** were obtained through 1,3-dipolar cycloaddition of bromonitrile oxide to alkenes (*S*)-**12** and (*R*)-**12**, respectively, as previously described [19]. Treatment of **5** with a 5:1 mixture of AcOH/H_2O provided alcohols **7a** and **7b** (Scheme 1A), that were separated by flash chromatography. Analog conditions led to the synthesis of alcohols **7c** and **7d**, starting from **6** (Scheme 1B). Alcohols **7a-d** were oxidized to the corresponding carboxylic acids **8a-d** using $Fe(NO_3)_3{\cdot}9H_2O$, TEMPO and KCl under an air flux, as O_2 source [20]. This is a cleaner method compared to traditional oxidation procedures used to convert alcohols into carboxylic acids, which typically involve the use of chromium-based reagents, and it allowed us to obtain the desired products in high yields (80-88%). The final amino acids **1a-d** were obtained after treatment of the *N*-Boc precursors (**8a-d**) with a 15% TFA solution in dichloromethane. The zwitterionic compounds were isolated after ion-exchange chromatography employing the DOWEX Marathon C (H^+ form) resin.

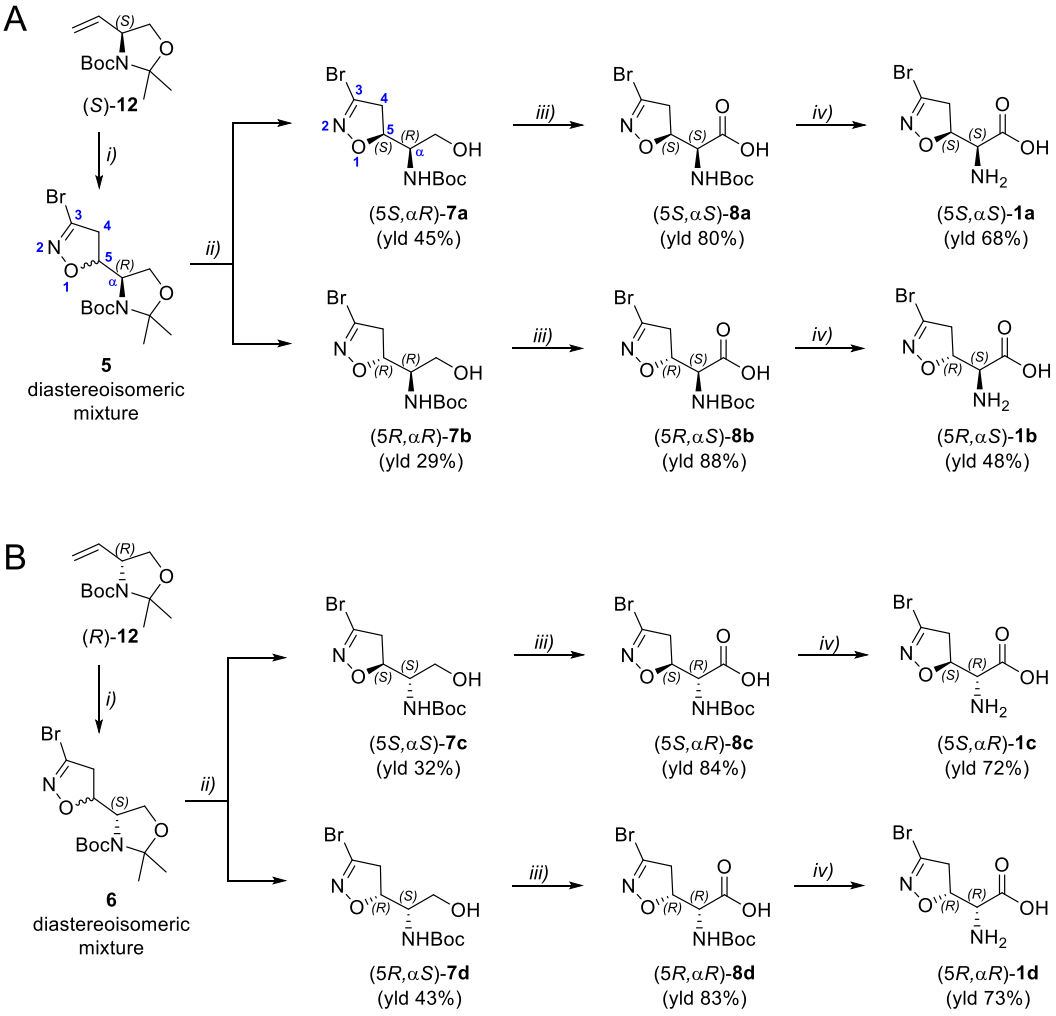

Scheme 1. (A, B) Synthesis of compounds **1a-1b** (A), and **1c-1d** (B). Reagents and conditions: *i)* according to Ref. [19]; *ii)* AcOH/H_2O 5:1, 40°C, 48h; *iii)* TEMPO, $Fe(NO_3)_3 \cdot 9H_2O$, KCl, air flux, DCE, r.t., 24h; *iv)* (1) 15% TFA, DCM, r.t., 1h; (2) column purification with Dowex Marathon C (H^+ form) resin, 10%Py/H_2O (eluent).

Compounds **2b-d**, **3b-d** and **4b-d** were synthesized following the procedure previously described for the (5*S*,α*S*) isomers **2a**, **3a** and **4a** [16]. Briefly, *N*-Boc protected carboxylic acids **8b-d** were treated with trimethylsylildiazomethane and methanol at room temperature to obtain the methyl esters **9b-d** (Scheme 2). Reaction of **8b-d** with benzylbromide under basic conditions at 50°C afforded benzyl esters **10b-d**. The coupling reaction between the carboxylic acids **8b-d** and benzylamine using EDC hydrochloride and HOBt gave amides **11b-d**. Intermediates **9b-d**, **10b-d** and **11b-d** were treated with a 15% TFA solution in dichloromethane to cleave the Boc-protecting group and give the free amines **2b-d**, **3b-d** and **4b-d**, respectively (Scheme 2).

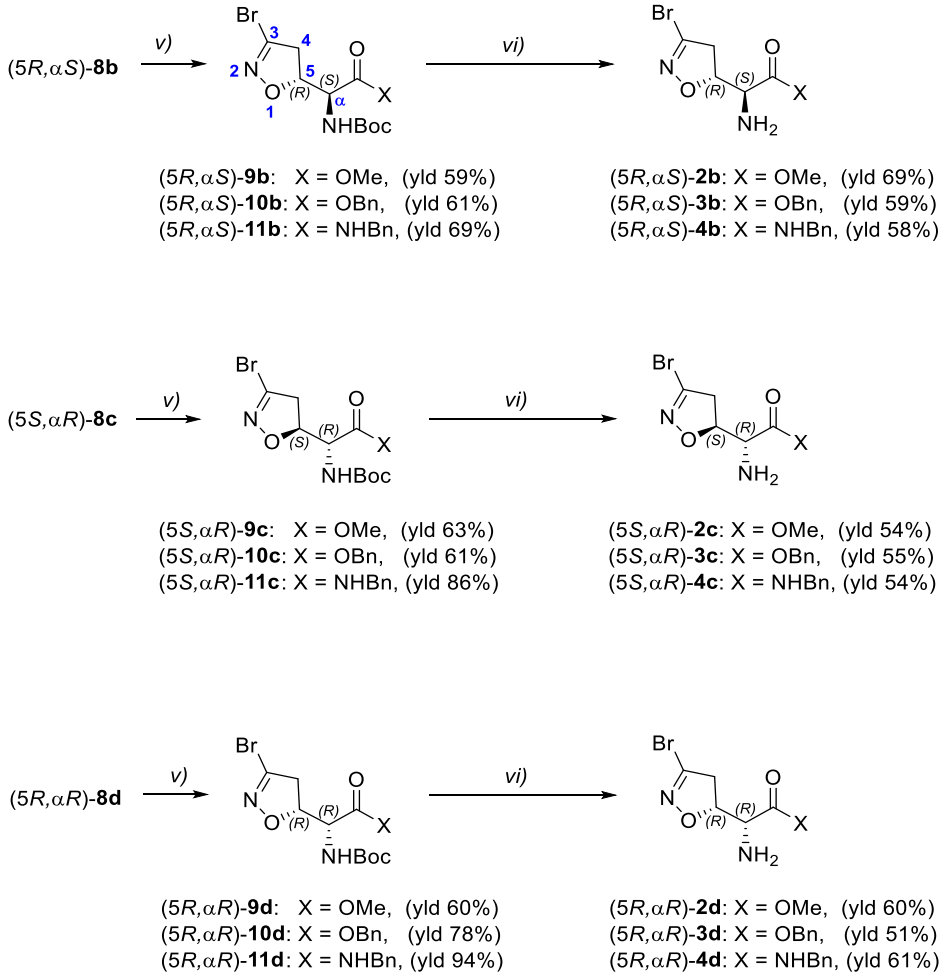

Scheme 2. (A, B) Synthesis of compounds **2b-d**, **3b-d** and **4b-d**. Reagents and conditions: *v)* 2N $TMSCHN_2$ in hexane, PhMe/MeOH, r.t., 1h (for **9**); BnBr, $KHCO_3$, DMF, 50°C, 1h (for **10**); $BnNH_2$, EDC·HCl, HOBt, dry THF, r.t., 2h (for **11**); *vi)* 15% TFA/DCM, r.t., 2-4h.

2.4. Antimalarial Activity against Plasmodium falciparum

All diastereoisomers were investigated for their *in vitro* antiplasmodial activity. The phenotypic assays were performed against D10 (chloroquine sensitive) and W2 (chloroquine resistant) *P. falciparum* strains, using the parasite lactate dehydrogenase (pLDH) method and chloroquine (CQ) as control. Considering all four compound subclasses (**1a-**

d, **2a-d**, **3a-d**, **4a-d**), the compounds showing the natural configuration (5*S*, *αS*) were significantly more active than the corresponding enantiomers and diastereoisomers. **1a-4a** showed submicromolar IC_{50}s against both *P. falciparum* strains (IC_{50} < 1 μM), with no significant differences between the two strains (D10 and W2, Table 1). While the natural (5*S*, *αS*) isomers (**1a-4a**) were potent antimalarial agents, the isomers possessing the (5*R*, *αR*) absolute configuration displayed a moderate antiplasmodial activity (1 < IC_{50} < 10 μM). The (5*S*, *αR*) and (5*R*, *αS*) absolute configurations resulted in a huge drop in the antimalarial potency, leading to poorly active compounds (Table 1).

Table 1. Chemical structures, clogD and IC_{50}s against *P. falciparum* D10 and W2 strains.

Structure	Compound	clogD[a]	*P.falciparum* D10 IC_{50} (μM)[b]	*P.falciparum* W2 IC_{50} (μM)[b]
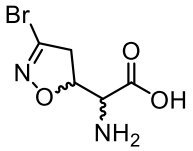	(5*S*, *αS*)-**1a**	0.02	0.35 ± 0.08	0.34 ± 0.12
	(5*R*, *αS*)-**1b**		23.54 ± 0.31	24.75 ± 0.90
	(5*S*, *αR*)-**1c**		7.49 ± 1.48	8.47 ± 2.06
	(5*R*, *αR*)-**1d**		8.79 ± 1.12	10.18 ± 1.75
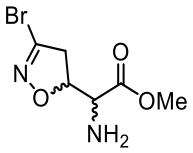	(5*S*, *αS*)-**2a**	0.04	0.79 ± 0.21	0.88 ± 0.23
	(5*R*, *αS*)-**2b**		17.14 ± 5.91	17.18 ± 7.39
	(5*S*, *αR*)-**2c**		40.67 ± 16.20	48.18 ± 14.81
	(5*R*, *αR*)-**2d**		8.27 ± 1.05	7.42 ± 3.54
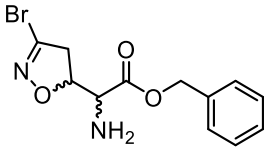	(5*S*, *αS*)-**3a**	1.41	0.37 ± 0.12	0.26 ± 0.05
	(5*R*, *αS*)-**3b**		32.65 ± 18.10	34.85 ± 5.30
	(5*S*, *αR*)-**3c**		19.35 ± 4.34	16.51 ± 8.11
	(5*R*, *αR*)-**3d**		4.31 ± 0.51	4.50 ± 1.82
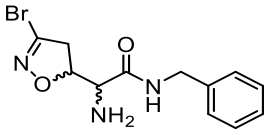	(5*S*, *αS*)-**4a**	0.76	0.36 ± 0.11	0.48 ± 0.18
	(5*R*, *αS*)-**4b**		18.20 ± 1.15	18.20 ± 0.93
	(5*S*, *αR*)-**4c**		19.35 ± 2.15	19.35 ± 3.36
	(5*R*, *αR*)-**4d**		8.55 ± 1.95	8.91 ± 3.40

[a]The clogD values (pH 7.4) were calculated by using ACD/pKa GALAS algorithm of ACD/Percepta software (ACD/Percepta, Advanced Chemistry Development, Inc., Toronto, ON, Canada, 2017, http://www.acdlabs.com.).
[b]pLDH method; data are the mean of three independent experiments ± SD; D10: CQ-susceptible *P. falciparum* strain; W2: CQ-resistant *P. falciparum* strain.

For the methyl ester derivatives, the enantiomer of **2a** [(5*R*, *αR*)-**2d**] was approximately 10-fold less potent than **2a** towards *P. falciparum* D10 and W2 strains, whereas the diastereoisomers (**2b** and **2c**) were inactive towards both strains (IC_{50} > 15 μM, Table 1). The same trend was observed for the other subclasses (**1a-d**, **3a-d** and **4a-d**), with the exception of **1c**, which presented an IC_{50} < 10 μM (Table 1). Thus, the stereochemistry led to significant differences in the antimalarial activity, with the natural isomers always being the most potent molecules. Since all isomers in each subclass (**1a-d**, **2a-d**, **3a-d** and **4a-d**) have the same clogD, the differences in antiplasmodial potency could not be correlated to a different passive diffusion across cell membranes. The natural compound (5*S*, *αS*) acivicin is known to compete with amino acids for cellular uptake via transporters. Indeed, acivicin uptake is mediated by the L-amino acid transport system that is responsible for the Na^+-independent transport of neutral amino acids [21,22]. The microenvironment of

P. falciparum-infected human erythrocytes is controlled by two membranes. Normal mature erythrocytes are relatively impermeable to L-Gln, and therefore also acivicin. The influx of L-Gln and other amino acids is controlled by different transporter systems, each varying their substrate specificity [23,24]. Our results suggested that the stereochemistry might be relevant for the recognition by the putative transporters, not only for the amino acid 3-BA (**1a**), but also for its ester and amide derivatives (**2a-4a**). Indeed, only the (5*S*, α*S*) natural isomers (**1a-4a**) showed a significant potency in inhibiting *P. falciparum* proliferation. To investigate whether the different antiplasmodial activities could be related also to a distinct interaction of the isomers with biological targets, we tested the inhibitory activity towards *Pf*GAPDH, which is a known target for **1a-4a** [16].

2.2. In vitro inhibitory activity towards PfGAPDH

3-Br-acivicin (**1a**) biological activity is correlated to its ability to inhibit multiple targets. Among these, *Pf*GAPDH had been previously suggested to be involved in the antimalarial effect of **1a** and other structurally related compounds [16]. For this reason, the four diastereoisomers of each compound were investigated for their ability to inhibit *Pf*GAPDH activity. All molecules were screened at a concentration of 100 μM, after a 3-hour incubation time. While 3-Br-acivicin (**1a**) produced a *Pf*GAPDH inhibition higher than 50%, its enantiomer **1d** and diastereoisomers (**1b** and **1c**) were inactive (Figure 2A). A similar trend was observed for the amide-bearing isomers **4a** compared to **4b-d**. In contrast, all four isomers of the methyl (**2a-d**) and benzyl (**3a-d**) ester derivatives were able to fully inhibit *Pf*GAPDH at a 100 μM concentration, leading to a residual *Pf*GAPDH activity lower than 1% (Figure 2A). Therefore, compounds **2a-d** and **3a-d** were selected for further investigation and tested at 50 μM for 30 minutes. All diastereoisomers (**2a-d** and **3a-d**) showed enzyme inhibition >50%, with the natural isomer **2a** being the most active (37% residual activity at 50 μM; Figure 2A).

The covalent mechanism of action of **2a** and **3a** had been already characterized though mass spectrometry, using undigested and trypsin-digested *Pf*GAPDH after incubation with the tested compounds [14]. We also proved the selective modification of the catalytic Cys153 with no involvement of other Cys residues [14]. In addition, the k_{inact}/K_i ratio typically used to characterize the covalent binding of irreversible inhibitors to the target protein was measured for compounds **1a-4a** [16]. Therefore, we can assume that the unnatural isomers **2b-4b**, **2c-4c** and **2d-4d** displayed the same irreversible mechanism of inhibition observed for their corresponding natural isomers (5*S*,α*S*) **1a-4a**.

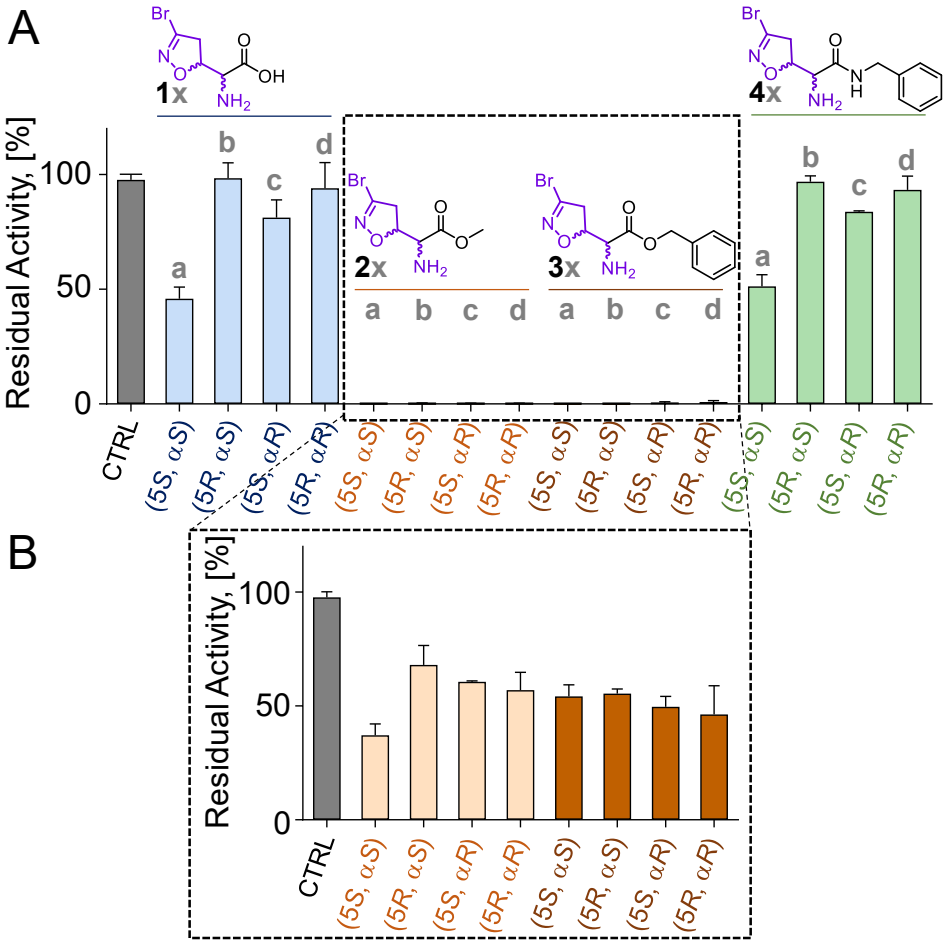

Figure 2. (**A**, **B**) Residual activity (%) of *Pf*GAPDH upon incubation with 100 μM of compounds **1a-d**, **2a-d**, **3a-d** and **4a-d** for 3 hours (A) or 50 μM of compounds **2a-d** and **3a-d** for 30 min (B). All experiments were performed at 25 °C in a buffered solution containing 10 mM TEA, 5 mM EDTA, 10 mM sodium arsenate, pH 7.6. *Pf*GAPDH was at 2 μM concentration. CTRL: activity of *Pf*GAPDH maintained under the same conditions in the absence of inhibitors. Experiments were performed in independent triplicates. Data are shown as mean ± SD.

2.3. Molecular modelling

Compounds **1a-1d**, **2b-2d**, **3b-3d**, **4b-4d** were subjected to conformational analysis and flexible docking simulations in complex with *Pf*GAPDH using the same computational procedure previously applied to **2a**, **3a**, and **4a** [16]. The present results (Table S1-S38) were integrated with those previously obtained, analyzed, and related to the inhibitory activities of the compounds. The aim was to simulate the binding of the compounds to *Pf*GAPDH just before undergoing the nucleophilic attack by the catalytic cysteine residue (C153). According to the flip-flop model proposed for the catalytic reaction mechanism of GAPDH, the substrate rotates around C153 moving the C-3 phosphate from a first (P_I) to a second (P_{II}) interaction site [25,26]. In line with these findings, different starting complexes were considered and two possible binding approaches to C153, named BA1 and BA2, were obtained for each compound, which corresponded to the approach from the P_I or P_{II} site, respectively (Figure 3 and 4; Tables S15-S32).

The geometry and the conformational energy of the docked ligands were compared to those of the conformers obtained by the conformational analysis (Table S33). The solvent-accessible surface (SASA) of the leaving group (bromine atom) was calculated (Table S34) and the ligand-protein interactions were analyzed (Table S35-S38).

It resulted that the active isomers **2a-2d** could approach C153 assuming both binding modes. In the BA1 (Figures 3A and S1), the protonated amine function and the ester function interacts with the P_I site while the bromine atom points towards NAD^+.

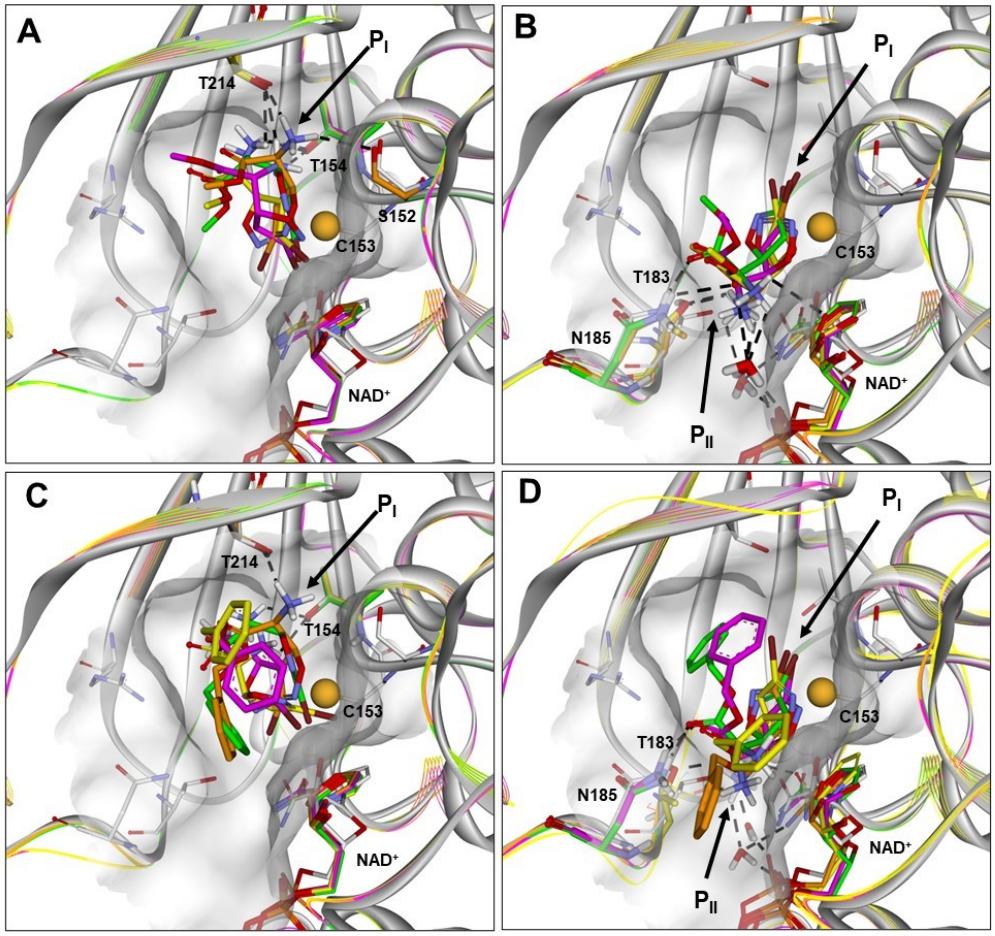

Figure 3. (**A**-**D**) Docked structures of *Pf*GAPDH in complex with: i) **2a** (orange), **2b** (yellow), **2c** (green) and **2d** (magenta) approaching from the P_I site (BA1; A) or P_{II} site (BA2; B); ii) **3a** (orange), **3b** (yellow), **3c** (green) and **3d** (magenta) approaching from the P_I site (BA1; C) or P_{II} site (BA2; D). All structures are superimposed on the starting *Pf*GAPDH conformation by fitting Cα atoms. The starting protein conformation (gray) is displayed as solid ribbons and the Connolly surface of the active site is shown. The backbone of the docked complexes is in line ribbons, key interaction residues are displayed and labelled, and heteroatoms are colored by atom type (N, blue; O, red; S, yellow; Br, brown). The van der Waals volume of the sulfur atom of C153 is scaled by 50%. Hydrogen atoms are omitted for clarity, except those involved in ligand-protein hydrogen bond interactions (black dashed lines).

In BA2 (Figures 3B and S2), the protonated amine and the ester function are located at the P_{II} site and the bromine atom is positioned at the P_I site pointing towards the active-site segment. Considering the orientation of the leaving group, this binding approach is favored by a larger solvent accessible surface area (SASA) of the bromine atom (Table S34). However, assuming the BA1 (Figures 3A and S1), the bromine atom could leave the active site together with NAD+, similarly to the hydride ion of the substrate. The putative binding conformations of **2a**-**2d** resulted all within 5 kcal/mol from the global energy minimum (GM) (Table S33).

Similar results were obtained for the active diastereoisomers **3a-3d** although characterized by a more hindered benzyl moiety compared to the methyl group of **2a-2d** (Figures 3C-D, S3 and S4). In particular, assuming the BA1, the phenyl ring is positioned in the large cleft between the S-loop (aa182-210) and the S7-S8 loop (aa122-130), being slightly

differently oriented according to the stereochemistry of the C5 carbon (occupying the P_{II} site in the 5*S* diastereoisomers **3a** and **3c**; Figure 3C). On the other hand, in the BA2, the phenyl ring is positioned according to the stereochemistry of the Cα carbon being oriented toward the P_I site or the P_{II} site in the α*R* (**3c**, **3d**) and α*S* (**3a**, **3b**) diastereoisomers, respectively (Figure 3D).

On the other hand, the results obtained for **1a-1d** suggest that a salt-bridge interaction between the negatively charged carboxylic group of the ligands and R237 of *Pf*GAPDH (involved in phosphate binding and translocation) could be responsible for the drastic reduction of the inhibitory activity of **1b**-**1d**. Indeed, when the carboxylic group is positioned at the P_I site (BA1; Figures 4A and S5), the salt-bridge with R237 is responsible for keeping the electrophilic carbon of the 3-bromo-4,5-dihydroisoxazole ring (C3) away from the sulfur atom of C153 (> 4 Å; **1b** and **1c**) or, in the case of **1d**, placing the 4,5-dihydroisoxazole nitrogen atom between the C3 carbon and the C153 sulphur atom. In any case, such ionic interaction hampers the approach to C153 and the formation of the carbon sulphur bond (~ 1.80 Å).

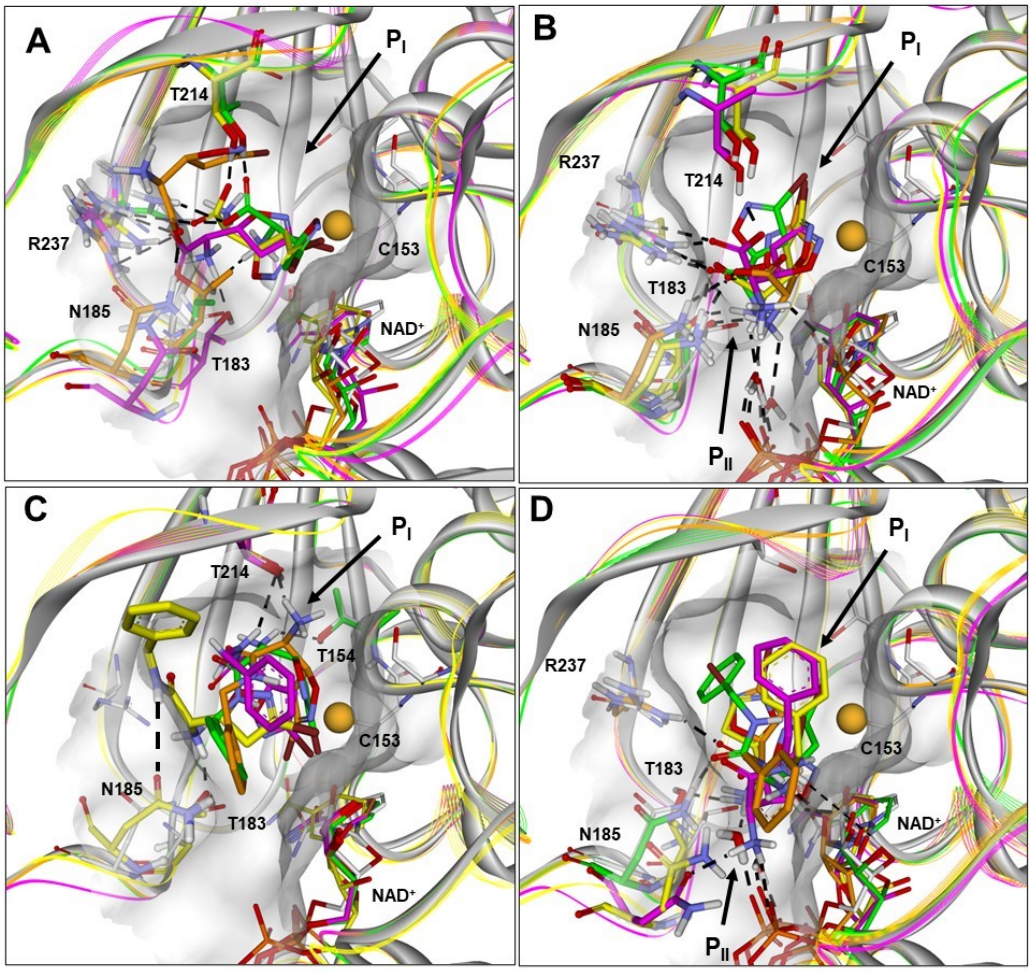

Figure 4. (**A-D**) Docked structures of *Pf*GAPDH in complex with: i) **1a** (orange), **1b** (yellow), **1c** (green) and **1d** (magenta) approaching from the P_I site (BA1; A) or P_{II} site (BA2; B); ii) **4a** (orange), **4b** (yellow), **4c** (green) and **4d** (magenta) approaching from the P_I site (BA1; C) or P_{II} site (BA2; D). All structures are superimposed on the starting *Pf*GAPDH conformation by fitting C*α* atoms. The starting protein conformation (gray) is displayed as solid ribbons and the Connolly surface of the active site is shown. The backbone of the docked complexes is in line ribbons, key interaction residues are displayed and labelled, and heteroatoms are colored by atom type (N, blue; O, red; S, yellow; Br, brown). The van der Waals volume of the sulfur atom of C153 is scaled by 50%. Hydrogen atoms are omitted for clarity, except those involved in ligand-protein hydrogen bond interactions (black dashed lines).

When the carboxylic group is positioned in the P_{II} site (BA2; Figures 4B and S6), the diastereoisomers **1b-1d** still present the salt-bridge with R237 together with a charge-assisted hydrogen bond interaction with T214, drastically reducing the SASA of the bromine atom positioned at P_I (Table S34). Importantly, the carboxylic group of **1a** (the only active diastereoisomer) is not involved in any interaction with R237 and, accordingly, the SASA of the bromine atom is not reduced (Tables S34 and S35). In line with what observed for the carboxylic group, for the amide derivatives **4b** and **4d**, the introduction of the NH group is responsible for additional interactions with the protein which move the ligand away from C153 (Figures 4C and 4D; Tables S27-S30; Figures S7 and S8). As previously reported, this is also true for **4a** (the only active diastereoisomer), but only assuming the BA2 [16]. Finally, diastereoisomer **4c** docked conformations are highly distorted in both binding approaches (Figures S9 and S10) and show an energy difference from the global minimum conformer higher than 15 kcal/mol (Table S33). Therefore, computational results are consistent with *Pf*GAPDH inhibitory activities and provide useful molecular models to drive future structural modifications.

3. Conclusions

Herein, we investigated the importance of stereochemistry for the biological activity of nature-inspired 3-Br-acivicin and its derivatives. For each molecule, the four isomers were prepared and evaluated *in vitro* towards *P. falciparum*. Only the (5*S*, α*S*) natural isomers showed a significant antimalarial activity, suggesting that their uptake might be mediated by the L-amino acid transport system. Considering the *Pf*GAPDH inhibition, the most potent compounds turned out to be the ester derivatives **2a-2d** and **3a-3d**, with no significant differences among the diastereoisomers. In contrast, stereochemistry affected target binding for the other two subclasses (**1a-1d** and **4a-4d**). A clear correlation between the *Pf*GAPDH inhibitory activity and the antimalarial potency was not observed, therefore additional targets might be involved in the biological effects. The racemic form of the 3-bromo-4,5-dihydroisoxazole scaffold had been exploited in chemoproteomic profiling methods to engage reactive cysteine residues in the human proteome [27]. Our enantiomerically pure 3-bromo-4,5-dihydroisoxazole derivatives represent valuable tools for proteomic experiments on malaria parasite *P. falciparum*, aiming to reveal new ligandable sites in proteins and to guide a future structure-based drug design.

4. Materials and Methods

4.1. Chemistry

4.1.1. General

All reagents, solvents and starting materials were purchased from Sigma-Aldrich, Fluorochem or TCI Europe. The diastereoisomeric mixtures **5** and **6** were prepared as previously described [19]. Compounds **2a**, **3a** and **4a** were prepared from intermediate **8a** as previously described [14,16]. ^{1}H NMR and ^{13}C NMR spectra were recorded with a Varian Mercury 300 (300 MHz) spectrometer. NMR spectra were obtained in deuterated solvents, such as $CDCl_3$ or D_2O. The chemical shift (δ values) are reported in ppm and corrected to the signal of the deuterated solvents. Peak multiplicities are reported as: s (singlet), d (doublet), dd (doublet of doublets), ddd (doublet of doublet of doublets), t (triplet), dt (doublet of triplets), q (quartet), m (multiplet), br (broadened). Chemical shifts (δ) are expressed in ppm and coupling constants (*J*) in Hertz (Hz). Thin layer chromatography (TLC) plates were purchased from Sigma-Aldrich (silica gel 60 F254 aluminum sheets, with fluorescence indicator 254 nm), a dilute alkaline solution of $KMnO_4$ or a ninhydrin solution were used to visualize the compounds. Flash chromatography was performed using silica gel, pore size 60 Å, 230-400 mesh particle size. Specific rotations ($[\alpha]_D^T$) were

calculated based on the optical rotation measurements obtained with a Jasco P1010 polarimeter coupled with a Haake N3-B thermostat.

4.1.2. General procedure A:

To a stirred solution of the appropriate *tert*-butyl (1-(3-bromo-4,5-dihydroisoxazol-5-yl)-2- hydroxyethyl)carbamate precursor **7a-d** (1 eq) in DCE (0.8 mL/mmol), KCl (0.1 eq), $Fe(NO_3)_3$ x $9H_2O$ (0.1 eq) and TEMPO (0.1 eq) were added. The reaction mixture was stirred under an air flow for 24 hours and the reaction progress was monitored by TLC. The solvent was evaporated and purification by silica gel column chromatography gave compounds **8a-d**.

4.1.3. General procedure B:

Compounds **8a-d** (1.0 eq) were treated with a 15% DCM solution of trifluoroacetic acid (10 eq) at 0 °C, and the solution was stirred at rt for 1 h. The volatiles were removed under vacuum and the crude was purified by ion-exchange chromatography using Dowex Marathon C (H^+ form) resin, elution with a 10% solution of pyridine in water. The solvent was evaporated under reduced pressure to obtain compounds **1a-d**.

4.1.4. General procedure C:

$TMSCHN_2$ 2.0 M in hexane (2 eq) was added dropwise to a cooled solution of **8b-d** (1 eq) in toluene (10 mL/mmol) and MeOH (0.4 mL/mmol). After stirring at room temperature for 1 h, the mixture was concentrated under reduced pressure and purification by silica gel column chromatography gave compounds **9b-d**.

4.1.5. General procedure D:

Compounds **8b-d** (1 eq) were dissolved in DMF (6 mL/mmol). Benzyl bromide (1.2 eq) and $KHCO_3$ (1.2 eq) were added to the solution. The reaction mixture was stirred at 50°C for 1 h. The reaction mixture was diluted with EtOAc and the organic layer was washed with 1N HCl, 5% $NaHCO_3$, and brine. The organic layer was dried over anhydrous Na_2SO_4, filtered, and evaporated to dryness. Purification by silica gel column chromatography gave compounds **10b-d**.

4.1.6. General procedure E:

Benzylamine (1 eq), EDC hydrochloride (1 eq) and HOBt (0.5 eq) were added to a solution of **8b-d** (1 eq) in dry THF (35 mL/mmol). The reaction mixture was stirred at room temperature for 2 h, then the solvent was removed under reduced pressure. Purification by silica gel column chromatography gave compounds **11b-d**.

4.1.7. General procedure F:

The *N*-Boc precursor **9b-d**, **10b-d** or **11b-d** (1 eq) was treated with a 15% DCM solution of trifluoroacetic acid (10 eq) at 0 °C. The resulting solution was stirred at rt for 4 h. The volatiles were removed under vacuum, 5% aqueous solution of $NaHCO_3$ was added, and the aqueous layer extracted with DCM. The organic layer was dried over anhydrous Na_2SO_4, filtered, and evaporated to dryness. Purification by silica gel column chromatography gave compounds **2b-d**, **3b-d** or **4b-d**.

*4.1.8. tert-Butyl ((R)-1-((S)-3-bromo-4,5-dihydroisoxazol-5-yl)-2-hydroxyethyl)carbamate (**7a**) and tert-butyl ((R)-1-((R)-3-bromo-4,5-dihydroisoxazol-5-yl)-2-hydroxyethyl)carbamate (**7b**)*

The diastereomeric mixture **5** (2.80 g, 8.02 mmol) was dissolved in a 5:1 mixture of $AcOH/H_2O$ (60 mL) and stirred at 40°C for 48 h. The solvent was evaporated and the crude

was dissolved in EtOAc and washed with water. Purification by silica gel column chromatography (cyclohexane/EtOAc 9:1) afforded I fraction **7a** (1.11 g, 3.61 mmol, 45% yield) and II fraction **7b** (719 mg, 2.33 mmol, 29% yield).

7a: white prisms (from *i*Pr$_2$O), $[\alpha]_D^{20}$ = +91.8 (c = 0.5, CHCl$_3$). ^{1}H NMR (300 MHz, CDCl$_3$) δ 5.11 (brs, 1H), 4.77 (ddd, *J* = 8.7, 8.7, 8.7, 1H), 3.88–3.99 (m, 1H), 3.67–3.82 (m, 2H), 3.25–3.38 (m, 2H), 1.89 (brs, 1H), 1.45 (s, 9H). ^{13}C NMR (75 MHz, Chloroform-*d*) δ 156.2, 138.5, 81.0, 80.5, 61.4, 54.2, 44.6, 28.5 (3C). Analytical data were in agreement with literature values [13].

7b: white prisms (from *i*Pr$_2$O), $[\alpha]_D^{20}$ = -91.5 (c = 0.5, CHCl$_3$). ^{1}H NMR (300 MHz, CDCl$_3$) δ 5.01–4.88 (m, 2H), 3.90-3.65 (m, 3H), 3.32 (dd, *J* = 17.5, 10.5 Hz, 1H), 3.21 (dd, *J* = 17.5, 8.4 Hz, 1H), 2.05 (brs, 1H), 1.45 (s, 9H). ^{13}C NMR (75 MHz, Chloroform-*d*) δ 156.5, 138.4, 80.9, 80.2, 62.3, 54.1, 43.9, 28.2 (3C).

*4.1.9. tert-Butyl ((S)-1-((S)-3-bromo-4,5-dihydroisoxazol-5-yl)-2-hydroxyethyl)carbamate (**7c**) and tert-butyl ((S)-1-((R)-3-bromo-4,5-dihydroisoxazol-5-yl)-2-hydroxyethyl)carbamate (**7d**)*

The diastereomeric mixture **6** (2.80 g, 8.02 mmol) was dissolved in a 5:1 mixture of AcOH/H$_2$O (60 mL) and stirred at 40°C for 48 h. The solvent was evaporated and the crude was dissolved in EtOAc and washed with water Purification by silica gel column chromatography (cyclohexane/EtOAc 9:1) afforded I fraction **7d** (1.07 g, 3.45 mmol, 43% yield) and II fraction **7c** (793 mg, 2.57 mmol, 32% yield).

7c: white prisms (from *i*Pr$_2$O), $[\alpha]_D^{20}$ = +90.1 (c = 0.5, CHCl$_3$). NMR data were consistent with those obtained for the corresponding enantiomer **7b**.

7d: white prisms (from *i*Pr$_2$O), $[\alpha]_D^{20}$ = -90.3 (c = 0.5, CHCl$_3$). NMR data were consistent with those obtained for the corresponding enantiomer **7a**.

*4.1.10. (S)-2-((S)-3-bromo-4,5-dihydroisoxazol-5-yl)-2-((tert-butoxycarbonyl)amino)acetic acid (**8a**)*

Compound **8a** was prepared according to general procedure A from intermediate **7a** (1.00 g, 3.23 mmol). Purification by silica gel column chromatography (cyclohexane/EtOAc 7:3 + 1% AcOH) gave compound **8a** as a white solid, which was recrystallized from *i*PrOH (836 mg, 2.59 mmol, 80% yield). $[\alpha]_D^{20}$ = +169.2 (c = 0.1, CHCl$_3$). ^{1}H NMR (300 MHz, CDCl$_3$) δ 5.45 (brs, 1H), 5.00 (ddd, *J*=11.0, 7.7, 3.9, 1H), 4.52 (dd, *J*=8.0, 3.9, 1 H), 3.30–3.60 (m, 2 H), 1.45 (s, 9H). Proton of COOH not seen. ^{13}C NMR (CDCl$_3$) δ 172.2, 155.7, 138.6, 82.1, 81.5, 56.3, 44.3, 28.5 (3C). Analytical data were in agreement with literature values [13].

*4.1.11. (S)-2-((R)-3-bromo-4,5-dihydroisoxazol-5-yl)-2-((tert-butoxycarbonyl)amino)acetic acid (**8b**)*

Compound **8b** was prepared according to general procedure A from intermediate **7b** (700 mg, 2.26 mmol). Purification by silica gel column chromatography (cyclohexane/EtOAc 7:3 + 1% AcOH) gave compound **8b** as a white solid, which was recrystallized from *i*PrOH (643 mg, 1.99 mmol, 88 % yield). $[\alpha]_D^{20}$ = -95.0 (c = 0.1, CHCl$_3$). ^{1}H NMR (300 MHz, CDCl$_3$) δ 5.31-5.22 (m, 2H), 4.58 (d, J = 9.3 Hz, 1H), 3.40 (dd, J = 17.7, 10.9 Hz, 1H), 3.25 (dd, J = 17.7, 7.7 Hz, 1H), 1.46 (s, 9H). Proton of COOH not seen. ^{13}C NMR (75 MHz, Methanol-*d*$_4$) δ 170.7, 157.1, 137.8, 81.4, 79.7, 55.8, 43.2, 27.2 (3C).

*4.1.12. (R)-2-((S)-3-bromo-4,5-dihydroisoxazol-5-yl)-2-((tert-butoxycarbonyl)amino)acetic acid (**8c**)*

Compound **8c** was prepared according to general procedure A from intermediate **7c** (700 mg, 2.26 mmol). Purification by silica gel column chromatography (cyclohexane/EtOAc 7:3 + 1% AcOH) gave compound **8c** as a white solid, which was recrystallized

from *i*PrOH (614 mg, 1.90 mmol, 84% yield). $[\alpha]_D^{20}$ = +98.0 (c = 0.1, $CHCl_3$). NMR data were consistent with those obtained for the corresponding enantiomer **8b**.

*4.1.13. (R)-2-((R)-3-bromo-4,5-dihydroisoxazol-5-yl)-2-((tert-butoxycarbonyl)amino)acetic acid (**8d**)*

Compound **8d** was prepared according to general procedure A from intermediate **7d** (1.00 g, 3.23 mmol). Purification by silica gel column chromatography (cyclohexane/EtOAc 7:3 + 1% AcOH) gave compound **8d** as a white solid, which was recrystallized from *i*PrOH (868 mg, 2.68 mmol, 83% yield). $[\alpha]_D^{20}$ = -168.5 (c = 0.1, $CHCl_3$). NMR data were consistent with those obtained for the corresponding enantiomer **8a**.

*4.1.14. (S)-2-amino-2-((S)-3-bromo-4,5-dihydroisoxazol-5-yl)acetic acid (**1a**)*

Compound **1a** was prepared according to general procedure B from intermediate **8a** (200 mg, 0.62 mmol). **1a** was obtained as a white solid, which was recrystallized from MeOH/H_2O (94 mg, 0.42 mmol, 68% yield). $[\alpha]_D^{20}$ = +172.2 (c = 0.1, water). ^{1}H NMR (300 MHz, D_2O) δ 5.08 (ddd, *J* = 11.0, 8.2, 3.3 Hz, 1H), 3.92 (d, *J* = 3.3 Hz, 1H), 3.45 (dd, *J* = 17.1, 11.0 Hz, 1H), 3.35 (dd, *J* = 17.1, 8.2 Hz, 1H). Protons of NH_2 and COOH not seen. ^{13}C NMR (75 MHz, D_2O) δ 170.0, 140.9, 79.7, 56.1, 42.9. Analytical data were in agreement with literature values [13].

*4.1.15. (S)-2-amino-2-((R)-3-bromo-4,5-dihydroisoxazol-5-yl)acetic acid (**1b**)*

Compound **1b** was prepared according to general procedure B from intermediate **8b** (200 mg, 0.62 mmol). **1b** was obtained as a white solid, which was recrystallized from MeOH/H_2O (66 mg, 0.30 mmol, 48% yield). $[\alpha]_D^{20}$ = -100.4 (c = 0.1, water). ^{1}H NMR (300 MHz, D_2O) δ 4.95 (ddd, *J* = 10.6, 7.5, 7.3 Hz, 1H), 3.77 (d, *J* = 7.3 Hz, 1H), 3.54 (dd, *J* = 18.3, 10.6 Hz, 1H), 3.40 (dd, *J* = 18.3, 7.5 Hz, 1H). Protons of NH_2 and COOH not seen. ^{13}C NMR (75 MHz, D_2O) δ 170.5, 140.8, 79.5, 56.4, 44.4.

*4.1.16. (R)-2-amino-2-((S)-3-bromo-4,5-dihydroisoxazol-5-yl)acetic acid (**1c**)*

Compound **1c** was prepared according to general procedure B from intermediate **8c** (200 mg, 0.62 mmol). **1c** was obtained as a white solid, which was recrystallized from MeOH/H_2O (99 mg, 0.45 mmol, 72% yield). $[\alpha]_D^{20}$ = +100.7 (c = 0.1, water). NMR data were consistent with those obtained for the corresponding enantiomer **1b**.

*4.1.17. (R)-2-amino-2-((R)-3-bromo-4,5-dihydroisoxazol-5-yl)acetic acid (**1d**)*

Compound **1d** was prepared according to general procedure B from intermediate **8d** (200 mg, 0.62 mmol). **1d** was obtained as a white solid, which was recrystallized from MeOH/H_2O (101 mg, 0.45 mmol, 73% yield). $[\alpha]_D^{20}$ = -170.4 (c = 0.1, water). NMR data were consistent with those obtained for the corresponding enantiomer **1a**.

*4.1.18. Methyl (S)-2-((R)-3-bromo-4,5-dihydroisoxazol-5-yl)-2-((tert-butoxycarbonyl)amino)acetate (**9b**)*

Compound **9b** was prepared according to general procedure C from intermediate **8b** (200 mg, 0.62 mmol). Purification by silica gel column chromatography (cyclohexane/EtOAc 8:2) gave compound **9b** as a yellow oil (123 mg, 0.37 mmol, 59% yield). $[\alpha]_D^{20}$ = -111.5 (c = 0.5, $CHCl_3$). ^{1}H NMR (300 MHz, Chloroform-*d*) δ 5.27-5.18 (m, 2H), 4.53 (dd, *J* = 9.4, 2.0 Hz, 1H), 3.81 (s, 3H), 3.36 (dd, *J* = 17.6, 10.8 *Hz*, 1H), 3.25 (dd, *J* = 17.6, 7.8 *Hz*, 1H) 1.46 (s, 9H). ^{13}C NMR (75 MHz, $CDCl_3$) δ 169.3, 156.2, 137.9, 81.4, 80. 8, 56.0, 53.0, 43.6, 28.2 (3C).

*4.1.19. Methyl (R)-2-((S)-3-bromo-4,5-dihydroisoxazol-5-yl)-2-((tert-butoxycarbonyl)amino)acetate (**9c**)*

Compound **9c** was prepared according to general procedure C from intermediate **8c** (200 mg, 0.62 mmol). Purification by silica gel column chromatography (cyclohexane/EtOAc 8:2) gave compound **9c** as a yellow oil (131 mg, 0.39 mmol, 63% yield). $[\alpha]_D^{20}$ = +113.9 (c = 0.5, $CHCl_3$). NMR data were consistent with those obtained for the corresponding enantiomer **9b**.

*4.1.20. Methyl (R)-2-((R)-3-bromo-4,5-dihydroisoxazol-5-yl)-2-((tert-butoxycarbonyl)amino)acetate (**9d**)*

Compound **9d** was prepared according to general procedure C from intermediate **8d** (200 mg, 0.62 mmol). Purification by silica gel column chromatography (cyclohexane/EtOAc 8:2) gave compound **9d** as a yellow oil (125 mg, 0.37 mmol, 60% yield). $[\alpha]_D^{20}$ = -156.4 (c = 0.5, $CHCl_3$). ^{1}H NMR (300 MHz, $CDCl_3$) δ 5.50 (d, *J* = 8.0, 1H), 4.92 (ddd, *J* = 10.5, 7.2, 3.3Hz, 1H), 4.42 (dd, *J* = 8.0, 3.3 Hz, 1H), 3.78 (s, 3H), 3.35–3.50 (m, 2H), 1.42 (s, 9H). ^{13}C NMR (75 MHz, $CDCl_3$) δ 169.3, 155.3, 138.2, 82.2, 80.9, 56.6, 53.2, 44.5, 28.4 (3C). NMR data were consistent with those reported in literature for the corresponding enantiomer **9a** [14].

*4.1.21. Benzyl (S)-2-((R)-3-bromo-4,5-dihydroisoxazol-5-yl)-2-((tert-butoxycarbonyl)amino)acetate (**10b**)*

Compound **10b** was prepared according to general procedure D from intermediate **8b** (200 mg, 0.62 mmol). Purification by silica gel column chromatography (cyclohexane/EtOAc 9:1) gave compound **10b** as a colourless oil (156 mg, 0.38 mmol, 61% yield). $[\alpha]_D^{20}$ = -99,8 (c = 0.5, $CHCl_3$). ^{1}H NMR (300 MHz, $CDCl_3$) δ 7.44 – 7.30 (m, 5H), 5.36 – 5.12 (m, 4H), 4.56 (dd, *J* = 9.5, 2.1 Hz, 1H), 3.34 (dd, J = 17.6, 10.7, 1H), 3.26 (dd, H = 17.6, 8.0, 1H), 1.45 (s, 9H). ^{13}C NMR (75 MHz, Chloroform-*d*) δ 169.3, 155.6, 138.0, 135.5, 128.9 (2C), 128.7 (2C), 128.6, 82.4, 80.8, 68.1, 57.4, 44.8, 28.6 (3C).

*4.1.22. Benzyl (R)-2-((S)-3-bromo-4,5-dihydroisoxazol-5-yl)-2-((tert-butoxycarbonyl)amino)acetate (**10c**)*

Compound **10c** was prepared according to general procedure D from intermediate **8c** (200 mg, 0.62 mmol). Purification by silica gel column chromatography (cyclohexane/EtOAc 9:1) gave compound **10c** as a colourless oil (156 mg, 0.38 mmol, 61% yield). $[\alpha]_D^{20}$ = +94.6 (c = 0.5, $CHCl_3$). NMR data were consistent with those obtained for the corresponding enantiomer **10b**.

*4.1.23. Benzyl (R)-2-((R)-3-bromo-4,5-dihydroisoxazol-5-yl)-2-((tert-butoxycarbonyl)amino)acetate (**10d**)*

Compound **10d** was prepared according to general procedure D from intermediate **8d** (200 mg, 0.62 mmol). Purification by silica gel column chromatography (cyclohexane/EtOAc 9:1) gave compound **10d** as a yellow oil (200 mg, 0.48 mol, 78% yield). $[\alpha]_D^{20}$ = -136.2 (c = 0.5, $CHCl_3$). ^{1}H NMR (300 MHz, $CDCl_3$) δ 7.30–7.40 (m, 5H), 5.55 (d, *J* = 6.0 Hz, 1H), 5.22 (d, *J* = 12.0 Hz, 1H), 5.14 (d, *J* = 12.0 Hz, 1H), 4.83 (ddd, *J* = 11.3, 6.9, 3.6 Hz, 1H), 4.50 (m, 1H), 3.42 (dd, *J* = 17.6, 6.9 Hz, 1H), 3.30 (dd, *J* = 17.6, 11.3 Hz, 1H), 1.42 (s, 9H). ^{13}C NMR (75 MHz, $CDCl_3$) δ 168.7, 155.3, 138.1, 134.9, 128.9 (2C), 128.9 (2C), 128.8, 82.3, 80.9, 68.3, 56.6, 44.4, 28.5 (3C). NMR data were consistent with those reported in literature for the corresponding enantiomer **10a** [14].

*4.1.24. tert-butyl ((S)-2-(benzylamino)-1-((R)-3-bromo-4,5-dihydroisoxazol-5-yl)-2-oxoethyl)carbamate (**11b**)*

Compound **11b** was prepared according to general procedure E from intermediate **8b** (200 mg, 0.62 mmol). Purification by silica gel column chromatography (cyclohexane/EtOAc 7:3) gave compound **11b** as a colourless oil (176 mg, 0.43 mmol, 69% yield). $[\alpha]_D^{20}$ = -97.7 (c = 1.0, $CHCl_3$). ^{1}H NMR (300 MHz, $CDCl_3$) δ 7.42 – 7.20 (m, 5H), 6.60 (brs, 1H), 5.43 – 5.19 (m, 2H), 4.57 – 4.27 (m, 3H), 3.37 (dd, *J* = 17.8, 11.1 Hz, 1H), 3.12 (dd, *J* =

17.8, 8.0 Hz, 1H), 1.44 (s, 9H). ^{13}C NMR (75 MHz, $CDCl_3$) δ 168.1, 155.8, 138.3, 137.4, 128.7 (2C), 127.7 (2C), 127.6, 80.8, 77.3, 56.2, 43.8, 43.6, 28.2 (3C).

*4.1.25. tert-butyl ((R)-2-(benzylamino)-1-((S)-3-bromo-4,5-dihydroisoxazol-5-yl)-2-oxoethyl)carbamate (**11c**)*

Compound **11c** was prepared according to general procedure E from intermediate **8c** (200 mg, 0.62 mmol). Purification by silica gel column chromatography (cyclohexane/EtOAc 7:3) gave compound **11c** as a colourless oil (219 mg, 0.53 mmol, 86% yield). $[\alpha]_D^{20}$ = +100.1 (c = 1.0, $CHCl_3$). NMR spectral data were in agreement with those of compound **11b**.

*4.1.26. tert-butyl ((R)-2-(benzylamino)-1-((R)-3-bromo-4,5-dihydroisoxazol-5-yl)-2-oxoethyl)carbamate (**11d**)*

Compound **11d** was prepared according to general procedure E from intermediate **8d** (200 mg, 0.62 mmol). Purification by silica gel column chromatography (cyclohexane/EtOAc 7:3) gave compound **11d** as a colourless oil (240 mg, 0.58 mmol, 94% yield). $[\alpha]_D^{20}$ = -138.7 (c = 1.0, $CHCl_3$). ^{1}H NMR (300 MHz, $CDCl_3$) δ 7.38-7.22 (m, 5H), 6.54 (t, *J* = 5.7 Hz, 1H), 5.48 (d, *J* = 7.8 Hz, 1H), 4.74 (ddd, *J* = 10.5, 8.3, 6.6 Hz, 1H), 4.48 (d, *J* = 5.7 Hz, 2H), 4.26 (dd, *J* = 8.3, 7.8 Hz, 1H), 3.52 (dd, *J* = 17.7, 6.6 Hz, 1H), 3.32 (dd, *J* = 17.7, 10.5 Hz, 1H), 1.44 (s, 9H). ^{13}C NMR (75 MHz, $CDCl_3$) δ 168.4, 155.9, 138.8, 137.4, 128.7 (2C), 127.6 (2C), 127.6, 81.8, 77.2, 55.7, 44.3, 43.8, 28.2 (3C). NMR data were consistent with those reported in literature for the corresponding enantiomer **11a** [16].

*4.1.27. Methyl (S)-2-amino-2-((R)-3-bromo-4,5-dihydroisoxazol-5-yl)acetate (**2b**)*

Compound **2b** was prepared according to general procedure F from intermediate **9b** (100 mg, 0.30 mmol, 1.0 eq). Purification by silica gel column chromatography (100% EtOAc) gave compound **2b** as a pale-yellow oil (49 mg, 0.20 mmol, 69% yield). $[\alpha]_D^{20}$ = -187.0 (c = 0.5, $CHCl_3$). ^{1}H NMR (300 MHz, $CDCl_3$) δ 5.07 (ddd, *J* = 10.7, 7.9, 3.4 Hz, 1H), 3.76 (s, 3H), 3.47 (d, *J* = 3.4 Hz, 1H), 3.40 (dd, *J* = 17.2, 7.9 Hz, 1H), 3.29 (dd, *J* = 17.2, 10.7 Hz, 1H), 1.70 (brs, 2H). ^{13}C NMR (75 MHz, $CDCl_3$) δ 172.8, 137.9, 82.2, 57.2, 52.6, 44.0.

*4.1.28. Methyl (R)-2-amino-2-((S)-3-bromo-4,5-dihydroisoxazol-5-yl)acetate (**2c**)*

Compound **2c** was prepared according to general procedure F from intermediate **9c** (100 mg, 0.30 mmol, 1.0 eq). Purification by silica gel column chromatography (100% EtOAc) gave compound **2c** as a pale-yellow oil (38 mg, 0.16 mmol, 54% yield). $[\alpha]_D^{20}$ = +184.3 (c = 0.5, $CHCl_3$). NMR spectral data were in agreement with those of compound **9b**.

*4.1.29. Methyl (R)-2-amino-2-((R)-3-bromo-4,5-dihydroisoxazol-5-yl)acetate (**2d**)*

Compound **2d** was prepared according to general procedure F from intermediate **9d** (100 mg, 0.30 mmol, 1.0 eq). Purification by silica gel column chromatography (100% EtOAc) gave compound **2d** as a colourless oil (42 mg, 0.18 mmol, 60% yield). $[\alpha]_D^{20}$ = -97.1 (c = 0.5, $CHCl_3$). ^{1}H NMR (300 MHz, $CDCl_3$) δ 5.00 (ddd, *J* = 10.7, 8.0. 3.5 Hz, 1H), 3.92 (d, *J* = 3.5 Hz, 1H), 3.75 (s, 3H), 3.33 (dd, *J* = 17.3, 8.0 Hz, 1H), 3.20 (dd, *J* = 17.3, 10.7 Hz, 1H), 1.80 (brs, 2H). ^{13}C NMR (75 MHz, $CDCl_3$) δ 172.0, 138.2, 82.7, 56.2, 52.8, 42.5.

NMR data were consistent with those reported in literature for the corresponding enantiomer **2a** [14].

*4.1.30. Benzyl (S)-2-amino-2-((R)-3-bromo-4,5-dihydroisoxazol-5-yl)acetate (**3b**)*

Compound **3b** was prepared according to general procedure F from intermediate **10b** (100 mg, 0.24 mmol, 1.0 eq). Purification by silica gel column chromatography (100% EtOAc) gave compound **3b** as an orange oil (45 mg, 0.14 mmol, 59% yield). $[\alpha]_D^{20}$ = -121.0 (c = 0.5, $CHCl_3$). ^{1}H NMR (300 MHz, $CDCl_3$) δ 7.49 – 7.30 (m, 5H), 5.22 (s, 2H), 5.13 (ddd, *J* = 10.9, 7.9, 3.4 Hz, 1H), 3.55 (d, *J* = 3.4 Hz, 1H), 3.43 (dd, *J* = 17.2, 7.9 Hz, 1H), 3.28 (dd, *J* =

17.2, 10.9 Hz, 1H), 1.90 (s, 2H). ^{13}C NMR (75 MHz, $CDCl_3$) δ 172.1, 137.9, 135.2, 128.7 (2C), 128.6 (2C), 128.4, 82.1, 67.5, 57.3, 44.0.

*4.1.31. Benzyl (R)-2-amino-2-((S)-3-bromo-4,5-dihydroisoxazol-5-yl)acetate (**3c**)*

Compound **3c** was prepared according to general procedure F from intermediate **10c** (100 mg, 0.24 mmol, 1.0 eq). Purification by silica gel column chromatography (100% EtOAc) gave compound **3c** as an orange oil (42 mg, 0.13 mmol, 55% yield). $[\alpha]_D^{20}$ = +122.9 (c = 0.5, $CHCl_3$). NMR spectral data were in agreement with those of compound **3b**.

*4.1.32. Benzyl (R)-2-amino-2-((R)-3-bromo-4,5-dihydroisoxazol-5-yl)acetate (**3d**)*

Compound **3d** was prepared according to general procedure F from intermediate **10d** (100 mg, 0.24 mmol, 1.0 eq). Purification by silica gel column chromatography (100% EtOAc) gave compound **3d** as an orange oil (39 mg, 0.12 mmol, 51% yield). $[\alpha]_D^{20}$ = -62.0 (c = 0.5, $CHCl_3$). ^{1}H NMR (300 MHz, $CDCl_3$) δ 7.40–7.30 (m, 5H), 5.21 (d, *J* = 12.0 Hz, 1H), 5.16 (d, *J* = 12.0 Hz, 1H), 4.98 (ddd, *J* = 10.7, 8.0, 3.9 Hz, 1H), 3.94 (d, *J* = 3.9 Hz, 1H), 3.33 (dd, *J* = 17.3, 8.0 Hz, 1H), 3.10 (dd, *J* = 17.3, 10.7 Hz, 1H), 1.60 (brs, 2H). ^{13}C NMR (75 MHz, $CDCl_3$) δ 171.4, 138.1, 135.3, 129.0 (2C), 128.9 (2C), 128.7, 82.8, 67.6, 56.3, 42.4. NMR data were consistent with those reported in literature for the corresponding enantiomer **3a** [14].

*4.1.33. (S)-2-amino-N-benzyl-2-((R)-3-bromo-4,5-dihydroisoxazol-5-yl)acetamide (**4b**)*

Compound **4b** was prepared according to general procedure F from intermediate **11b** (150 mg, 0.36 mmol, 1 eq). Purification by silica gel column chromatography (100% EtOAc) gave compound **4b** as a white solid (66 mg, 0.21 mmol, 58% yield). m.p. = 122-123°C. $[\alpha]_D^{20}$ = -112.7 (c = 1.0, $CHCl_3$). ^{1}H NMR (300 MHz, $CDCl_3$) δ 7.71 (brs, 1H), 7.52 – 7.13 (m, 5H), 5.11 – 4.78 (m, 1H), 4.57 – 4.31 (m, 2H), 3.51 (d, *J* = 5.8 Hz, 1H), 3.50-3.40 (m, 2H), 1.86 (brs, 2H). ^{13}C NMR (75 MHz, $CDCl_3$) δ 171.1, 138.4, 138.0, 128.7 (2C), 127.6 (2C), 127.5, 82.5, 57.6, 44.2, 43.3.

*4.1.34. (R)-2-amino-N-benzyl-2-((S)-3-bromo-4,5-dihydroisoxazol-5-yl)acetamide (**4c**)*

Compound **4c** was prepared according to general procedure F from intermediate **11c** (150 mg, 0.36 mmol, 1 eq). Purification by silica gel column chromatography (100% EtOAc) gave compound **4c** as a white solid (61 mg, 0.20 mmol, 54% yield). $[\alpha]_D^{20}$ = +110.2 (c = 1.0, $CHCl_3$). NMR spectral data were in agreement with those of compound **4b**.

*4.1.35. (R)-2-amino-N-benzyl-2-((R)-3-bromo-4,5-dihydroisoxazol-5-yl)acetamide (**4d**)*

Compound **4d** was prepared according to general procedure F from intermediate **11d** (150 mg, 0.36 mmol, 1 eq). Purification by silica gel column chromatography (100% EtOAc) and recrystallization from iPrOH/n-hexane gave compound **4c** as colourless needles (69 mg, 0.22 mmol, 61% yield). $[\alpha]_D^{20}$ = -79.0 (c = 1.0, $CHCl_3$). ^{1}H NMR (300 MHz, $CDCl_3$) δ 7.41-7.23 (m, 6H), 5.09 (dt, *J* = 9.6, 4.8 Hz, 1H), 4.44 (d, *J* = 6.3 Hz, 2H), 3.80 (d, *J* = 4.8 Hz, 1H), 3.22 (d, *J* = 9.6 Hz, 2H), 1.60 (brs, 2H). ^{13}C NMR (75 MHz, $CDCl_3$) δ 170.6, 138.1, 137.8, 128.8 (2C), 127.7 (2C), 127.7, 82.8, 56.4, 43.3, 41.8. NMR data were consistent with those reported in literature for the corresponding enantiomer **4a** [16].

4.2. Molecular modeling

Molecular modeling calculations were performed on CPU/GPU hybrid High Performance Computing Cluster (10 Twin servers, for a total of 560 Intel® Xeon® Gold processors (128 GB RAM), 64 AMD® EPYC® processors and 2 GPU NVIDIA® Tesla® V100) and on High Performance Computing Cluster (6 Twin servers s for a total of 12 nodes each equipped with Intel® Xeon® QuadCore E5520 CPU, 36 GB RAM). The molecular modeling graphics were carried out on personal computer equipped with Intel(R) Core (TM) i7-8700 processor and SGI Octane 2 workstations.

The apparent pKa and clogD values (pH 7.4) of compounds **1a-1d**, **2a-2d**, **3a-3d** and **4a-4d** were calculated by using ACD/pKa GALAS algorithm of ACD/Percepta software (ACD/Percepta, Advanced Chemistry Development, Inc., Toronto, ON, Canada, 2017, http://www.acdlabs.com.). Then, the percentage of neutral/ionized forms was computed at pH 7.2 (cytoplasm pH value) using the Handerson−Hasselbalch equation.

4.2.1. Conformational analysis

The molecular models of new compounds of **1a-1d**, **2b-2d**, **3b-3d** and **4b-4d** were built (Small Molecule tool of Discovery Studio 2017; Dassault Systèmes BIOVIA, San Diego, 2017), atomic potentials and charges were assigned using the CFF forcefield [28]. Resulting structures were subjected to molecular mechanic (MM) energy minimization (ε = 80*r) until the maximum RMS derivative was less than 0.001 kcal/Å, using Conjugate Gradient as minimization algorithm [29]. The obtained conformers were used as starting structures for the subsequent systematic conformational analysis (Search Small Molecule Conformations; Discovery Studio 2017). The conformational space was sampled by systematically varying the rotatable bonds sp3-sp3 and sp3-sp2 with an increment of 60°. The RMSD cutoff for structure selection was set to 0.01 (Å). Finally, to ensure a wide variance of the input structures to be successively fully minimized, an energy threshold value of 10^6kcal/mol was used as selection criteria. The generated structures were then subjected to MM energy minimization (CFF forcefield; ε = 80*r) until the maximum RMS derivative was less than 0.001 kcal/Å, using Conjugate Gradient as minimization algorithm. Finally, the resulting conformers were ranked by their potential energy values (i.e., ΔE from the global energy minimum). The conformers within 5 kcal/mol from the global minimum were classified on the basis of dihedral angle values.

4.2.2. Docking studies

Docking calculations were performed by using as protein structure the previously developed atomic model of *Pf*GAPDH [16]. Although in the docking simulation all the systems is perturbed by a Monte Carlo/minimization procedure, nevertheless the docking procedure formally requires a reasonable starting structure. In order to define the starting conformation of the new compounds, all the conformers within 5 kcal/mol from the global minimum were placed in GAPDH catalytic site considering the two binding modes of the glyceraldehyde 3-phosphate analogue 2-(2-phosphono-ethyl)-acrylic acid 4-nitro-phenyl ester (PDB ID: 1ML3). The conformations with the lowest potential energy that did not show significant steric overlap with catalytic-site amino acids were selected as starting conformations for the docking calculations.

A docking procedure, which considers all the systems as flexible (i.e., ligand and protein), was applied. Flexible docking was achieved using the Affinity module in the Insight 2005 suite, setting the SA_Docking procedure [30] and using the Cell Multipole method for non-bonded interactions [31]. The docking procedure included a Monte Carlo (MC) based conformational search of the ligand within the active site of *Pf*GAPDH. During the first step, starting from the previously obtained roughly docked structures, the ligand was moved by a random combination of translation, rotation, and torsional changes to sample both the conformational space of the ligand and its orientation with respect to the protein (MxRChange = 3 Å; MxAngChange = 180°). During this step, van der Waals (vdW) and Coulombic terms were scaled to a factor of 0.1 to avoid very severe divergences in the vdW and Coulombic energies. If the energy of a complex structure resulting from random moves of the ligand was higher by the energy tolerance parameter than the energy of the last accepted structure, it was not accepted for minimization. To ensure a wide variance of the input structures to be successively minimized, an energy tolerance value of 10^6 kcal/mol from the previous structure was used. After the energy minimization step (conjugate gradient; 2500 iterations; ε = 1), the energy test, with an energy range of 50 kcal/mol, and a structure similarity check (rms tolerance = 0.3 kcal/Å) was applied to select the 20

acceptable structures. Each subsequent structure was generated from the last accepted structure.

All *Pf*GAPDH atoms were left free to move during the entire course of docking calculations, whereas, in order to avoid unrealistic results, a tethering restraint was applied on Structurally Conserved Regions (SCRs) of the protein. To identify SCRs, the *Pf*GAPDH sequence was analyzed using the Structure Prediction and Sequence Analysis server PredictProtein (http://www.predictprotein. org/). In *Pf*GAPDH, 8 α-helix and 16 β-sheet secondary structures were predicted to be highly conserved (α1, aa13−23; α2, aa40−48; α3, aa105−113; α4, aa155−167; α5, aa198−207; α6, aa214−227; α7, aa258-270; α8, aa323-335 β1, aa4-8; β2, aa29-34; β3, aa58−62; β4, aa66−70; β5, aa73−79; β6, aa93-98; β7, aa118-123; β8, aa131-136; β9, aa146-149; β10, aa171-182; β11, aa234-238; β12, aa244-252; β13, aa275-278; β14, aa296-299; β15, aa303-306; β16, aa310-317). Within the identified SCRs, the distance between backbone hydrogen bond donors and acceptors in the α-helices was restrained within 2.5 Å. On the other hand, the φ and ψ torsional angles of the β-sheets were restrained within -119° and +113°, or -139° and +135°, respectively, according to the parallel or anti-parallel structure. According to the reliability index values obtained from the secondary structure prediction analysis, we applied restraints with a quadratic form and the following set of force constants: i) 1 kcal/mol/Å^2 (maximum force: 10 kcal/mol/Å^2) for reliability index values from 0 to 3, ii) 10 kcal/mol/Å^2 (maximum force: 100 kcal/mol/Å^2) for reliability index values from 4 to 6, and iii) 100 kcal/mol/Å^2 (maximum force: 1000 kcal/mol/Å^2) for reliability index values from 7 to 9. Moreover, in order to investigate the first approach of our compounds to the catalytic site before the nucleophilic attack, a tethering restraint was applied on: i) the hydrogen bond between the catalytic residues C153 and H180 (constrained within 2.5 Å using a force constant of 100 (kcal/mol)/Å) and ii) the distance between the electrophilic carbon of the 3-bromo-4,5-dihydroisoxazole ring and the sulfur atom of C153 (constrained within 3.4 Å using a force constant of 100 (kcal/mol)/Å according to the data present in the literature) [32,33].

For each compound, the resulting complexes were superimposed on the starting structure by fitting all the Cα atoms, and the Cα RMSD of each residue and its average value were calculated. Then, the complexes were again superimposed on the starting structure by fitting the Cα atoms of the residues characterized by an average value of RMSD ≤ 0.2 Å. Considering this latter superimposition, the Cα RMSD of the catalytic residues and the RMSD of NAD$^+$ were calculated. The χ1 torsion angle of C153 and the geometric criteria of the hydrogen bond between C153 and H180 were also evaluated for each generated complex. In particular, the angle D-H-A and X-D-A of this hydrogen bond was calculated assuming as D the sulfur atom of C153, as A the Nτ hydrogen atom of H180 and as X the Cβ of C153.

Finally, for each generated complex, the non-bonded interaction energy (vdW and electrostatic energy contribution; Group Based method [34]; CUT_OFF = 100; ε = 2*r; Discover_3 Module of Insight2005) was calculated. In our previous publication, the docked complexes of **2a**, **3a** and **4a** were not analyzed using these criteria [16]. Accordingly, to properly compare the results obtained for new diastereoisomers with those obtained with **2a**, **3a** and **4a**, these latter were also included in this analysis.

For each docking calculation, the complex with the most favorable interaction energy and characterized by i) Cα RMSD of C152 and H179 with respect to the starting structure ≤ 3 Å; ii) the gauche(-) conformation (from -30° to -90°) of the torsion angle χ1 of C153 (i.e., the conformation needed to establish the hydrogen bond with H180) iii) the angles of the hydrogen bond between C153 and H180 > 90° [35] was selected.

The selected docked complexes were then subjected to MM energy minimization applying only the restraint on the hydrogen bond between the catalytic residues C153 and H180 (RMS derivative < 0.5 kcal/Å; Steepest Descent algorithm; ε = 80*r; Module Discover; Insight 2005). The optimized complexes were again filtered by the using in addition to the above reported criteria the distance between the electrophilic carbon C3 of the 3-bromo-4,5-dihydroisoxazole ring and the sulfur atom of C153 ≤ 4 Å.

The complex with the most favorable interaction energy meeting the filtering criteria was chosen as the structure representing the most probable calculated approach of the compounds to the catalytic cysteine of *Pf*GAPDH. The quality of the selected docked complexes was checked using Procheck structure evaluator software [36].

4.3. Biological assays

4.3.1. Expression and purification of PfGAPDH

Recombinant His-tagged *Pf*GAPDH was produced in *Escherichia coli*, as already described [14].

4.3.2. Enzyme assays

GAPDH activity was evaluated using a modified version of the Ferdinand assay5 in a buffered solution containing 10 mM TEA, 10 mM sodium arsenate, 5 mM EDTA, 1.5 mM NAD^+ and 2.2 mM DL-glyceraldehyde 3-phosphate, as already described [14]. GAPDH was added at a final concentration of 33 nM and NADH formation was monitored at 340 nm using a Cary4000 spectrophotometer (Agilent Technologies) with the cell holder maintained at 25 °C.

4.3.3. Parasite growth and drug susceptibility assay

The CQ sensitive (D10) and CQ resistant (W2) strains of *P. falciparum* were sustained in vitro as described by Trager and Jensen [37,38]. All strains were cultured at 5% hematocrit (human type A-positive red blood cells) in RPMI 1640 (EuroClone, Celbio) medium with the addition of 1% AlbuMax (Invitrogen, Milan, Italy), 0.01% hypoxanthine, 20 mM Hepes Buffer, and 2 mM glutamine. Parasites were maintained at 37 °C in a standard gas mixture consisting of 1% O_2, 5% CO_2, and 94% N_2. For the drug sensitivity assay, compounds were dissolved in DMSO and then diluted with medium to achieve the required concentrations (final DMSO concentration <1%, which is nontoxic to the parasite). Drugs were placed in 96 well flat-bottom microplates (COSTAR) and serial dilutions made. Asynchronous cultures with parasitemia of 1–1.5% and 1% final hematocrit were added into the plates and incubated for 72 h at 37 °C. Parasite growth was determined spectrophotometrically (OD650) by measuring the activity of the parasite lactate dehydrogenase (pLDH), according to a modified version of Makler's method in control and drug-treated cultures [39]. Antiplasmodial activity is expressed as the 50% inhibitory concentrations (IC_{50}). Each IC_{50} value is the mean ± standard deviation of at least three separate experiments performed in duplicate.

Supplementary Materials: molecular modelling data (Table S1-S38; Figure S1-S10) are available online.

Author Contributions: Conceptualization: A.G., P.C.; methodology and investigation: A.G., A.Z., A.I.C., M.P., O.T., S.Bo., N.B., S.P.; data interpretation: A.G., C.B., P.C.; visualization and manuscript writing: C.B., P.C.; supervision: L.T., C.F., S.Br., N.B., S.P., P.C. All authors have read and agreed to the published version of the manuscript.
[#]A.G. and A.Z. contributed equally.

Acknowledgments: We thank the UNIMI GSA-IDEA project for promoting networking activities and collaborations that were fundamental for this work. C.B. thanks L'Oréal Italy for Women and Science in collaboration with Italy's National Commission for UNESCO for the "L'Oréal Italia for Women in Science" fellowship.

Conflicts of Interest: The authors declare no conflict of interest.

References

1. Atanasov, A.G.; Zotchev, S.B.; Dirsch, V.M.; Supuran, C.T. Natural products in drug discovery: advances and opportunities. *Nat Rev Drug Discov* **2021**, *20*, 200-216, doi:10.1038/s41573-020-00114-z.

2. Saldívar-González, F.I.; Aldas-Bulos, V.D.; Medina-Franco, J.L.; Plisson, F. Natural product drug discovery in the artificial intelligence era. *Chem Sci* **2022**, *13*, 1526-1546, doi:10.1039/d1sc04471k.
3. Nelson, A.; Karageorgis, G. Natural product-informed exploration of chemical space to enable bioactive molecular discovery. *RSC Med Chem* **2021**, *12*, 353-362, doi:10.1039/d0md00376j.
4. A, N.L.B.; F, M.D.S.; Batista, J.M.; Cass, Q.B. Enantiomeric mixtures in natural product chemistry: separation and absolute configuration assignment. *Molecules* **2018**, *23*, 492, doi:10.3390/molecules23020492.
5. Scott, K.A.; Ropek, N.; Melillo, B.; Schreiber, S.L.; Cravatt, B.F.; Vinogradova, E.V. Stereochemical diversity as a source of discovery in chemical biology. *Current Research in Chemical Biology* **2022**, *2*, 100028, doi:https://doi.org/10.1016/j.crchbi.2022.100028.
6. Elder, F.C.T.; Feil, E.J.; Snape, J.; Gaze, W.H.; Kasprzyk-Hordern, B. The role of stereochemistry of antibiotic agents in the development of antibiotic resistance in the environment. *Environment International* **2020**, *139*, 105681, doi:https://doi.org/10.1016/j.envint.2020.105681.
7. Miles, B.W.; Thoden, J.B.; Holden, H.M.; Raushel, F.M. Inactivation of the amidotransferase activity of carbamoyl phosphate synthetase by the antibiotic acivicin. *J Biol Chem* **2002**, *277*, 4368-4373, doi:10.1074/jbc.M108582200.
8. Denton, J.E.; Lui, M.S.; Aoki, T.; Sebolt, J.; Weber, G. Rapid in vivo inactivation by acivicin of CTP synthetase, carbamoyl-phosphate synthetase II, and amidophosphoribosyltransferase in hepatoma. *Life Sci* **1982**, *30*, 1073-1080, doi:10.1016/0024-3205(82)90527-6.
9. Earhart, R.H.; Neil, G.L. Acivicin in 1985. *Adv Enzyme Regul* **1985**, *24*, 179-205, doi:10.1016/0065-2571(85)90076-7.
10. Williams, K.; Cullati, S.; Sand, A.; Biterova, E.I.; Barycki, J.J. Crystal structure of acivicin-inhibited gamma-glutamyltranspeptidase reveals critical roles for its C-terminus in autoprocessing and catalysis. *Biochemistry* **2009**, *48*, 2459-2467, doi:10.1021/bi8014955.
11. Chittur, S.V.; Klem, T.J.; Shafer, C.M.; Davisson, V.J. Mechanism for acivicin inactivation of triad glutamine amidotransferases. *Biochemistry* **2001**, *40*, 876-887, doi:10.1021/bi0014047.
12. Galbiati, A.; Zana, A.; Conti, P. Covalent inhibitors of GAPDH: From unspecific warheads to selective compounds. *Eur J Med Chem* **2020**, *207*, 112740, doi:10.1016/j.ejmech.2020.112740.
13. Conti, P.; Pinto, A.; Wong, P.E.; Major, L.L.; Tamborini, L.; Iannuzzi, M.C.; De Micheli, C.; Barrett, M.P.; Smith, T.K. Synthesis and in vitro/in vivo evaluation of the antitrypanosomal activity of 3-bromoacivicin, a potent CTP synthetase inhibitor. *ChemMedChem* **2011**, *6*, 329-333, doi:10.1002/cmdc.201000417.
14. Bruno, S.; Pinto, A.; Paredi, G.; Tamborini, L.; De Micheli, C.; La Pietra, V.; Marinelli, L.; Novellino, E.; Conti, P.; Mozzarelli, A. Discovery of covalent inhibitors of glyceraldehyde-3-phosphate dehydrogenase, a target for the treatment of malaria. *J Med Chem* **2014**, *57*, 7465-7471, doi:10.1021/jm500747h.
15. van Niekerk, D.D.; Penkler, G.P.; du Toit, F.; Snoep, J.L. Targeting glycolysis in the malaria parasite Plasmodium falciparum. *Febs j* **2016**, *283*, 634-646, doi:10.1111/febs.13615.
16. Cullia, G.; Bruno, S.; Parapini, S.; Margiotta, M.; Tamborini, L.; Pinto, A.; Galbiati, A.; Mozzarelli, A.; Persico, M.; Paladino, A.; et al. Covalent inhibitors of Plasmodium falciparum glyceraldehyde 3-phosphate dehydrogenase with antimalarial activity in vitro. *ACS Med Chem Lett* **2019**, *10*, 590-595, doi:10.1021/acsmedchemlett.8b00592.
17. Bruno, S.; Margiotta, M.; Pinto, A.; Cullia, G.; Conti, P.; De Micheli, C.; Mozzarelli, A. Selectivity of 3-bromo-isoxazoline inhibitors between human and Plasmodium falciparum glyceraldehyde-3-phosphate dehydrogenases. *Bioorg Med Chem* **2016**, *24*, 2654-2659, doi:10.1016/j.bmc.2016.04.033.
18. Pacchiana, R.; Mullappilly, N.; Pinto, A.; Bova, S.; Forciniti, S.; Cullia, G.; Dalla Pozza, E.; Bottani, E.; Decimo, I.; Dando, I.; et al. 3-Bromo-isoxazoline derivatives inhibit GAPDH enzyme in PDAC cells triggering autophagy and apoptotic cell death. *Cancers (Basel)* **2022**, *14*, 3153, doi:10.3390/cancers14133153.

19. Pinto, A.; Conti, P.; De Amici, M.; Tamborini, L.; Madsen, U.; Nielsen, B.; Christesen, T.; Bräuner-Osborne, H.; De Micheli, C. Synthesis and pharmacological characterization at glutamate receptors of the four enantiopure isomers of tricholomic acid. *J Med Chem* **2008**, *51*, 2311-2315, doi:10.1021/jm701394a.
20. Jiang, X.; Zhang, J.; Ma, S. Iron catalysis for room-temperature aerobic oxidation of alcohols to carboxylic acids. *J Am Chem Soc* **2016**, *138*, 8344-8347, doi:10.1021/jacs.6b03948.
21. Huber, K.R.; Rosenfeld, H.; Roberts, J. Uptake of glutamine antimetabolites 6-diazo-5-oxo-L-norleucine (DON) and acivicin in sensitive and resistant tumor cell lines. *Int J Cancer* **1988**, *41*, 752-755, doi:10.1002/ijc.2910410519.
22. Maeda, K.; Nakajima, Y.; Motoyama, T.; Kitou, Y.; Kosaki, T.; Saito, T.; Nishiuchi, T.; Kanamaru, K.; Osada, H.; Kobayashi, T.; et al. Effects of acivicin on growth, mycotoxin production and virulence of phytopathogenic fungi. *Lett Appl Microbiol* **2014**, *59*, 377-383, doi:10.1111/lam.12289.
23. Elford, B.C. L-Glutamine influx in malaria-infected erythrocytes: a target for antimalarials? *Parasitol Today* **1986**, *2*, 309-312, doi:10.1016/0169-4758(86)90126-2.
24. Kirk, K. Membrane transport in the malaria-infected erythrocyte. *Physiol Rev* **2001**, *81*, 495-537, doi:10.1152/physrev.2001.81.2.495.
25. Moniot, S.; Bruno, S.; Vonrhein, C.; Didierjean, C.; Boschi-Muller, S.; Vas, M.; Bricogne, G.; Branlant, G.; Mozzarelli, A.; Corbier, C. Trapping of the thioacylglyceraldehyde-3-phosphate dehydrogenase intermediate from Bacillus stearothermophilus. Direct evidence for a flip-flop mechanism. *J Biol Chem* **2008**, *283*, 21693-21702, doi:10.1074/jbc.M802286200.
26. Cook, W.J.; Senkovich, O.; Chattopadhyay, D. An unexpected phosphate binding site in glyceraldehyde 3-phosphate dehydrogenase: crystal structures of apo, holo and ternary complex of Cryptosporidium parvum enzyme. *BMC Struct Biol* **2009**, *9*, 9, doi:10.1186/1472-6807-9-9.
27. Byun, D.P.; Ritchie, J.; Holewinski, R.; Kim, H.-R.; Tagirasa, R.; Ivanic, J.; Weekley, C.M.; Parker, M.W.; Adresson, T.; Yoo, E. Covalent inhibition by a natural product-inspired latent electrophile. *bioRxiv* **2023**, 2023.01.16.524242, doi:10.1101/2023.01.16.524242.
28. Ewig, C.S.; Berry, R.; Dinur, U.; Hill, J.R.; Hwang, M.J.; Li, H.; Liang, C.; Maple, J.; Peng, Z.; Stockfisch, T.P.; et al. Derivation of class II force fields. VIII. Derivation of a general quantum mechanical force field for organic compounds. *J Comput Chem* **2001**, *22*, 1782-1800, doi:10.1002/jcc.1131.
29. Fletcher, R. Unconstrained optimization. In *Practical Methods of Optimization*; John Wiley & Sons Ltd: New York, NY, USA, 1980; Volume 1, pp. 1–128.
30. Senderowitz, H.; Guarnieri, F.; Still, W.C. A Smart Monte Carlo Technique for Free Energy Simulations of multiconformational molecules. Direct calculations of the conformational populations of organic molecules. *Journal of the American Chemical Society* **1995**, *117*, 8211-8219, doi:10.1021/ja00136a020.
31. Ding, H.Q.; Karasawa, N.; III, W.A.G. Atomic level simulations on a million particles: The cell multipole method for Coulomb and London nonbond interactions. *The Journal of Chemical Physics* **1992**, *97*, 4309-4315, doi:10.1063/1.463935.
32. Lodola, A.; Branduardi, D.; De Vivo, M.; Capoferri, L.; Mor, M.; Piomelli, D.; Cavalli, A. A catalytic mechanism for cysteine N-terminal nucleophile hydrolases, as revealed by free energy simulations. *PLoS One* **2012**, *7*, e32397, doi:10.1371/journal.pone.0032397.
33. Arafet, K.; Ferrer, S.; Gonzalez, F.V.; Moliner, V. Quantum mechanics/molecular mechanics studies of the mechanism of cysteine protease inhibition by peptidyl-2,3-epoxyketones. *Phys Chem Chem Phys* **2017**, *19*, 12740-12748, doi:10.1039/c7cp01726j.
34. Steinbach, P.J.; Brooks, B.R. New spherical-cutoff methods for long-range forces in macromolecular simulation. *Journal of Computational Chemistry* **1994**, *15*, 667-683, doi:https://doi.org/10.1002/jcc.540150702.

35. Baker, E.N.; Hubbard, R.E. Hydrogen bonding in globular proteins. *Prog Biophys Mol Biol* **1984**, *44*, 97-179, doi:10.1016/0079-6107(84)90007-5.
36. Laskowski, R.A.; MacArthur, M.W.; Moss, D.S.; Thornton, J.M. PROCHECK: a program to check the stereochemical quality of protein structures. *Journal of Applied Crystallography* **1993**, *26*, 283-291, doi:doi:10.1107/S0021889892009944.
37. Imperatore, C.; Persico, M.; Aiello, A.; Luciano, P.; Guiso, M.; Sanasi, M.F.; Taramelli, D.; Parapini, S.; Cebrián-Torrejón, G.; Doménech-Carbó, A.; et al. Marine inspired antiplasmodial thiazinoquinones: synthesis, computational studies and electrochemical assays. *RSC Advances* **2015**, *5*, 70689-70702, doi:10.1039/C5RA09302C.
38. Trager, W.; Jensen, J.B. Human malaria parasites in continuous culture. *Science* **1976**, *193*, 673-675, doi:10.1126/science.781840.
39. Makler, M.T.; Hinrichs, D.J. Measurement of the lactate dehydrogenase activity of Plasmodium falciparum as an assessment of parasitemia. *Am J Trop Med Hyg* **1993**, *48*, 205-210, doi:10.4269/ajtmh.1993.48.205.

TOC

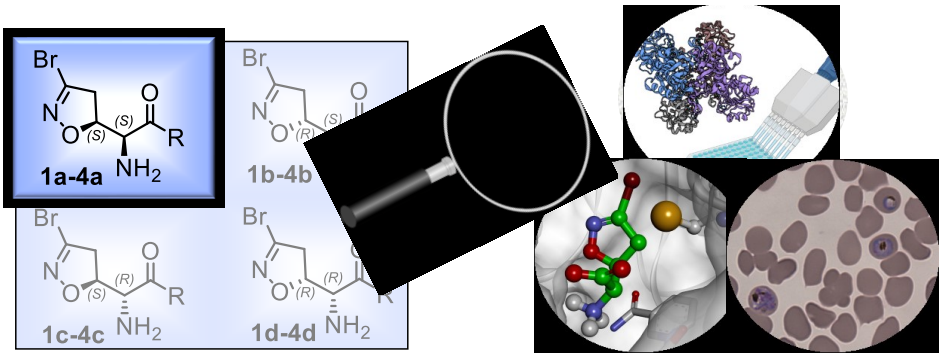
Br
N
O
(S)
(S)
O
R
NH2
1a-4a
Br
N
O
(R)
(S)
O
1b-4b
Br
N
O
(S)
(R)
O
R
NH2
1c-4c
Br
N
O
(R)
(R)
NH2
1d-4d